表 1. 術前因子

	全 例 (n=45)	S群 (n=23)	L群 (n=22)	p 値
平均年齢 (歳)	73.3±9.7	75.6± 7.6	70.9±11.1	NS
術前弁輪径 (mm)	19.7±2.3	18.2± 1.0	21.2± 2.3	<0.0001
BSA (m^2)	1.5±0.2	1.4± 0.2	1.59± 0.2	0.0009
術前 PG (mmHg)	84.7±29.0	93.4±31.1	75.5±24.0	0.0376
緊急例	6例 (13.3%)	5例 (21.7%)	1例 (4.5%)	0.0899
術前 AVA (cm^2)	0.7±0.3	0.6± 0.3	0.9± 0.2	0.0003
術前 NYHA 分類 (度)	2.2±1.0	2.3± 1.0	2.1± 0.9	NS
術前 LVDd (mm)	46.4±8.1	43.7± 6.4	49.3± 8.8	0.0182
術前 LVDs (mm)	28.9±9.1	27.8± 7.3	30.1±10.7	NS

PG=pressure gradient

表 2. 術中・術後因子

	全 例	S群	L群	p 値
人工弁サイズ (mm)	20.4±2.1	19.3±1.5	21.5±2.1	0.0003
supra-annular	8例 (17.8%)	6例 (26.1%)	2例 (9.1%)	NS
intra-annular	37例 (82.2%)	17例 (73.9%)	20例 (90.9%)	NS
体外循環時間 (分)	170.8±48.1	174.7±52.3	166.8±44.0	NS
大動脈遮断時間 (分)	123.1±37.8	126.3±43.6	119.5±30.9	NS
術後 PG (mmHG)	30.0±12.3	31.1±13.2	29.0±11.5	NS
術後 LVDd (mm)	43.7±8.1	41.0±7.4	46.3±8.2	0.0317
術後 LVDs (mm)	28.1±8.9	26.0±7.6	30.1±9.7	NS
術後 AVA (cm^2)	1.6±0.6	1.5±0.6	1.6±0.7	NS
術後 NYHA 分類 (度)	1.1±0.3	1.1±0.3	1.1±0.3	NS
在院日数	26.4±10.0	24.3±9.6	28.7±10.1	NS
死 亡	1例 (2.2%)	0	1例 (4.5%)	NS

砕した石灰片は，ハンドピースの先端部位から吸引される．十分に弁輪部組織の脱灰を行い，左室内の小ガーゼを除去した後に生理食塩水 300 ml にて洗浄した．人工弁は原則として 70 歳未満であれば機械弁を，それ以上では生体弁を使用することとした．また，人工弁の縫着は原則として水平マットレス縫合による intra-annular position とした．

本法により AVR を行った症例に対し，術前因子として New York Heart Association (NYHA) 分類，体表面積 (BSA)，心エコーによる大動脈弁輪径と心機能，および弁口面積 (AVA) を検討した．また術中・術後因子として，挿入した人工弁の大きさと挿入位置，人工心肺時間，術後心エコーによる心機能評価，在院日数，転帰について検討した．

以上の項目に関して，術前心エコーにおける弁輪径が 19 mm 未満 (S群) とそれ以上 (L群) との 2 群に分け，統計学的検討を行った．また，狭小弁輪を有する S群に関しては，NYHA 分類と心エコー結果の術前後における変化に関して検討を行った．

統計学的評価は，各測定項目を平均値±標準偏差で示し，両群間の有意差検定には χ^2 検定と Student t 検定を用いた．$p<0.05$ を統計学的に有意と判定した．

II. 結　　果

1. 全例 (n=45) [表 1, 2]

術前の BSA は 1.5±0.2 m^2，NYHA 分類は 2.2±1.0 度であった．心エコーにおける平均弁輪径 19.7±2.3 mm，左室拡張末期径 (LVDd)

46.4±8.1 mm，左室収縮末期径（LVDs）28.9±9.1 mm，AVA 0.7±0.3 cm²で，大動脈弁圧較差（PG）は84.7±29.0 mmHgであった．手術で挿入した人工弁のサイズは20.4±2.1 mmであり，37例（82.2%）でintra-annular positionに挿入した．術後に行った心エコー結果では弁周囲逆流はなく，平均AVA 1.6±0.6 cm²，平均PG 30.0±12.3 mmHgであった．平均在院日数は26.4±10.0日で，手術死亡は1例（2.2%）であった．

2．S群（n=23）とL群（n=22）

1）術前因子：S群の弁輪径は18.2±1.0 mm，BSAも1.4±0.2 m²で，AVAもL群と比べて有意に小さかった．また，術前PGはS群のほうが有意に高く，LVDdは有意に小さかった．

2）術中・術後因子：人工弁サイズは，S群は19.3±1.5 mmとL群の21.5±2.1に対して有意に小さかったが，人工弁の挿入位に関しては両群間で有意差はなかった．また，術後のLVDdは術前同様にS群で有意に小さかった．その他のPGやAVA，NYHA分類，転帰に関しては，両群間に有意差を認めなかった．

3．S群の術前後におけるNYHAおよび心エコー結果（表3）

術前の弁輪径18.2±1.0 mmに対し，術後の人工弁サイズは19.3±1.5 mmと有意に拡大した．また，PGやAVA，LVDd，NYHA分類は有意に改善した．LVDsのみ有意差を認めなかった．

表3．S群における術前後検査所見

	術前	術後	p値
弁輪径（mm）	18.2± 1.0	19.3± 1.5	0.0031
PG（mmHg）	93.4±31.1	31.1±13.2	<0.0001
AVA（cm²）	0.6± 0.3	1.5± 0.6	<0.0001
NYHA分類（度）	2.3± 1.0	1.1± 0.3	<0.0001
LVDd（mm）	43.7± 6.4	41.0± 7.4	0.0159
LVDs（mm）	27.8± 7.3	26.0± 7.6	NS

III．考　　察

弁の石灰化が著しいASでは，弁輪部の石灰化が残存すると弁周囲逆流の原因となったり，適切なサイズの人工弁を挿入することが困難となるため，石灰除去がきわめて重要である．これまでにも超音波手術器を用い石灰化を除去してAVRを行った方法は報告されている[1~3]が，当科では2002年1月から同様な機器であるSonopetを用いてAVRを行ってきた．本機器は超音波による石灰の破砕・脱灰機能とハンドピース先端からの吸引機能，およびイリゲーション機能をもつ超音波手術機器である．ハンドピースの発振周波数は25 kHzであり，操作性がよいアングルハンドピースを用いた．先端部は2～2.5 mmと弁輪部における手技にあった太さである．また，先端部位から破砕された石灰片を吸引でき，術中の塞栓予防に寄与する．

実際の脱灰の方法であるが，可及的に弁を切除した後に，石灰化部位にチップをあてながら，一点に集中しないように石灰部を削いだり掃いたりするように動かすことが組織の破壊を予防し，安全に石灰化除去を行ううえで重要である．

45例全例で本法を施行することができ，手技中に弁輪部が過剰に破壊されたり組織を損傷することはなく，破砕・脱灰した石灰が飛散して除去に困ることもなかった．また，弁輪部石灰化が著しい症例では十分な弁輪径が確保できず，supra-annular positionでのAVRをせざるをえない場合がある．しかし，自験例では37例（82.2%）で水平マットレス縫合が可能であった．これは，本法により弁輪部が十分に拡大され，かつ組織に柔軟性が出たためと考えられた．術後に弁周囲逆流を認めた症例はなく良好な結果を得たこと，また手技が簡便で時間がかからないことから，有用な方法であると考えられた．

術前に計測した弁輪径が19 mm未満の狭小弁輪を有する症例では，手術を行うにあたりどのくらいの大きさの人工弁が挿入できるかが問題となる．狭小弁輪例に対してはManouguian法[4,5]やNicks法[6]，Konno法[7]などの弁輪拡大術が報告されている．しかし，成人AS例で狭小弁輪を有する症例は高齢者やBSAが小さい症例であることが多く，弁輪拡大術は脆弱な組織や硬化組織に対する術式となる．また，最近では19 mmの機械弁を用いたAVRの良好な成績[8]や，狭小弁に

対するCarpentier-Edwards pericardial valve (Edwards Lifesciences社，アーバイン) を用いたAVRにおける良好な成績[9]などが本邦で報告されていることから，実際には弁輪拡大術の施行を躊躇することがある．

自験例では，術前に19 mm未満の狭小弁輪を有すると診断されたS群において，手術により挿入した人工弁サイズは19.3±1.5 mmと，術前の弁輪径18.2±1.0 mmと比べて有意に大きなサイズの人工弁を挿入しえた．S群におけるBSAは1.4±0.2 m²と，これまでの報告[8,9]と同様に小さく，術後の心エコー結果や経過も良好であったことから，S群における人工弁のサイズは妥当であったと考えられた．またS群・L群間の検討では，弁の位置，術後の安静時PGやNYHA分類，予後に有意差はなく，良好な結果を得られた．

以上より，術前に狭小弁輪と診断されていても，症例によってはSonopetを用いて石灰除去を行うことで，弁輪拡大術を行わずに弁輪部の拡大効果が期待できることから，本法は容易かつ安全な石灰化弁輪拡大法であると考えられた．

おわりに

AVRにおける石灰化弁輪に対し，Sonopetを用いて石灰除去を行った．本法は安全かつ容易に適切な大きさの人工弁を挿入することが可能であり，有用な石灰化弁輪拡大法であると考えられた．

文　献

1) McBride LR, Naunheim KS, Fiore AC et al : Aortic valve decalcification. J Thorac Cardiovasc Surg 100 : 36-43, 1990
2) Sheppard BB, Milliken JC, Nelson RJ et al : Ultrasonic decalcification of the aortic annulus during aortic valve replacement. Ann Thorac Surg 52 : 59-65, 1991
3) Unal M, Sanisoglu I, Konuralp C et al : Ultrasonic decalcification of calcified valve and annulus during heart valve replacement. Tex Heart Inst J 23 : 85-87, 1996
4) Manouguian S : A new method for patch enlargement of hypoplastic aortic annulus ; an experimental study (author's transl). Thoraxchir Vask Chir 24 : 418-423, 1976
5) Manouguian S, Seybold-Epting W : Patch enlargement of the aortic valve ring by extending the aortic incision into the anterior mitral leaflet ; new operative technique. J Thorac Cardiovasc Surg 78 : 402-412, 1979
6) Nicks R, Cartmill T, Berustein L : Hypoplasia of the aortic root ; the problem of aortic valve replacement. Thorax 25 : 339-346, 1970
7) Konno S, Imai Y, Iida Y et al : A new method for prosthetic valve replacement in congenital aortic stenosis associated with hypoplasia of the aortic valve ring. J Thorac Cardiovasc Surg 70 : 909-917, 1975
8) 伊藤　智，川人宏次，田中正史ほか：狭小大動脈弁に対する19 mm二葉弁の遠隔成績．日心臓血管外会誌 34 : 167-171, 2005
9) 古川貢之，桑原正知，中村栄作ほか：Carpentier Edwards pericardial valve 19 mm, 20 mmを用いた大動脈弁置換術の術後血行動態の検討．日心臓血管外会誌 32 : 240-242, 2003

SUMMARY

Aortic Valve Replacement for Calcified Aortic Valve and Annulus with Ultrasonic Decalcification

Keita Kikuchi et al., Department of Cardiovascular & General Surgery, Shimane University Faculty of Medicine, Izumo, Japan

We conducted ultrasonic decalcification on calcified annulus in patients with aortic stenosis (AS) using an ultrasonic operator, Sonopet (UST-2001) prior to aortic valve replacement (AVR). We studied the reliability of this method.

Subject and method : From January 2002 to August 2005, AVR was conducted for AS using the Sonopet in 45 patients, comprising of 18 male and 27 female subjects. The mean age was 73.3±9.7.

Result : Artificial valves were successfully inserted at the intra-annular level in 37 patients and at the supra-annular level in 8 patients without conducting annular enlargement. In the patients with narrow annuli of less than 19 mm (23 patients), the preoperative mean annular diameter was 18.2±1.0 mm, but significantly larger artificial valves with an average diameter of 19.3±1.5 mm

($p=0.003$) were successfully inserted.

Conclusion : AVR was proved to be safe and easy by previous ultrasonic decalcification of the annuls using the Sonopet. This method was very useful because it required no enlargement of aortic annulus.

KEY WORDS : small aortic annulus/aortic stenosis/ultrasonic surgical system/aortic root enlargement/ultrasonic decalcification

*　　*　　*

Blind Subxiphoid Pericardiotomy for Cardiac Tamponade Because of Acute Hemopericardium

Yoshihiko Kurimoto, MD, Mamoru Hase, MD, Satoshi Nara, MD, Naoya Yama, MD, Nobuyoshi Kawaharada, MD, Kiyofumi Morishita, MD, Tetsuya Higami, MD, and Yasufumi Asai, MD

Objective: Percutaneous catheter drainage (PCD) is not always effective in a case of hemopericardium. Acute occlusion of catheter and cardiac perforation can happen more often. To perform subxiphoid pericardiotomy within a minute for emergency cases, we have done this procedure in a blind method after finger dissection by subxiphoid approach. We report the usefulness of blind subxiphoid pericardiotomy (BSP) based on the results of a prospective control study.

Methods: We designed a study to determine a favorable management for cardiac tamponade resulting from hemopericardium. In an emergency case of cardiac tamponade because of hemopericardium, board certified surgeons should perform BSP and other emergency physicians should perform PCD, with or without local anesthesia. PCD (n = 67) and BSP (n = 16) were performed for patients with cardio-pulmonary arrest (CPA) or near CPA because of cardiac tamponade secondary to trauma (n = 7), acute aortic dissection (n = 65), and cardiac rupture following acute myocardial infarction (n = 11) in our emergency medical center from January 2000 to December 2004.

Results: BSP was effective in all cases but PCD was ineffective in five cases because of clotting in pericardium ($p = 0.260$). No complication was observed in the BSP group but five critical complications and three infeasible drainage complications were observed in the PCD group ($p = 0.146$). Ten patients (BSP, 4; PCD, 6; $p = 0.077$) survived after emergency surgery (n = 8) or conservative treatment (n = 2).

Conclusion: BSP was safe and could be performed quickly in an emergency situation. Percutaneous catheter drainage for hemopericardium could not avoid critical complications because of clotting in pericardium.

Key Words: Pericardiotomy, Pericardiocentesis, Hemopericardium, Cardiac tamponade.

J Trauma. 2006;61:582–585.

Cardiac tamponade caused by acute hemopericardium is critical and requires emergency intervention. Based on the clinical course and the findings of echo-free space in a pericardial sac, an initial treatment should be performed for relief of cardiac tamponade as early as possible. Many reports have supported the usefulness of percutaneous pericardial catheter drainage (PCD) against pericardial effusion.[1–3] PCD is less invasive, which seems preferable for severely ill patients. However, hemopericardium is different from pericardial effusion because of the possibility of clot in the pericardial sac and usually the hemopericardium becomes critical in a short period.[4,5] Conventional subxiphoid pericardiostomy overcomes some drawbacks of PCD, but requires specialized surgical instruments and takes several minutes to accomplish. We have employed subxiphoid pericardiotomy in a blind manner for selected cases with cardiopulmonary arrest (CPA) or near CPA because of cardiac tamponade caused by hemopericardium to quickly relieve the cause of CPA. In this prospective control study, we evaluate the results of blind subxiphoid pericardiotomy (BSP) for cardiac tamponade because of acute hemopericardium and compare them with the result of PCD.

Submitted for publication March 17, 2006.

Accepted for publication June 26, 2006.

From the Departments of Traumatology and Critical Care Medicine (Y.K., M.H., S.N., Y.A.), Thoracic and Cardiovascular Surgery (N.K., K.M., T.H.), and Radiology (N.Y.), Sapporo Medical University, Sapporo, Japan.

Presented as a poster at the 64th Annual Meeting of the American Association for the Surgery of Trauma September 22–24, 2005, Atlanta, Georgia.

Address for reprints: Yoshihiko Kurimoto, MD, Department of Traumatology and Critical Care Medicine, Sapporo Medical University, South 1 West 16, Chuo-ku, Sapporo 060-8543, Japan; email: kurimoto@sapmed.ac.jp.

DOI: 10.1097/01.ta.0000236060.37952.ce

METHODS

We designed a prospective control study to determine the preferred initial treatment for cases with CPA or near CPA because of cardiac tamponade caused by acute hemopericardium. In our emergency medical center, it was decided that board certified surgeons should perform BSP and other emergency physicians should perform PCD to relieve cardiac tamponade caused by acute hemopericardium. Eighty-three patients were admitted and given a diagnosis of cardiac tamponade because of acute hemopericardium as the cause of CPA or near CPA from January 2000 to December 2004. Sixty-nine patients suffered CPA during transportation to the hospital and the remaining 14 patients suffered CPA or near CPA after arrival at our emergency room. PCD (n = 67) and BSP (n = 16) were performed for patients with cardiac tamponade secondary to trauma (n = 7), acute aortic dissection (n = 65) and cardiac rupture after acute myocardial infarction (n = 11). There was no difference statistically between the two groups (Table 1).

BSP

Most patients had been undergoing cardiopulmonary resuscitation (CPR) with tracheal intubation before or during BSP. A 5 cm-long skin incision is made from the lower end

Table 1 Patients' Characteristics

	No.	Age	Male/ Female	Trauma/ AD/MI	CPAOA/ CPAAA
PCD	67	70.4 ± 15.7	30/37	6/54/7	59/8
BSP	16	66.5 + 16.4	9/7	1/11/4	10/6

PCD, percutaneous pericardial catheter drainage; BSP, blind subxiphoid pericardiotomy; AD, aortic dissection; MI, myocardial infarction; CPAOA, cardiopulmonary arrest on arrival; CPAAA, cardiopulmonary arrest (or near CPA) after arrival.

of the sternum caudally. The upper linea alba is divided in the midline without resection of the xiphoid sternum (Fig. 1A). The tissue plane between the posterior wall of the sternum and the anterior pericardium is developed by blunt finger dissection without any specific surgical instrument (Fig. 1B). While touching the pericardium with an index finger, an inferior site of the pericardium is cut by scissors (Fig. 1C). If cardiac tamponade is not quickly relieved by pericardiotomy, clots in the pericardium are evacuated using a suction system. In cases in which spontaneous circulation is restored, a drainage tube (20–28 Fr.) is placed in the pericardium (Fig. 1D) and a skin incision is approximated temporarily to transport patients to an operating room if indicated.

Percutaneous Pericardial Catheter Drainage

Most patients had been undergoing CPR with tracheal intubation before or during PCD. After confirmation of distance and direction from the subxiphoid access site to the pericardium using echocardiography, the pericardium is entered with an 18-gauge needle by a standard subxiphoid approach. A 0.035-in (0.089 cm) J tip guide wire is advanced into the pericardial space and the needle removed. The tract of the needle is dilated with an 8.5 Fr. dilator, and an 8.5 Fr. pericardial catheter (Pericardiocentesis set, Cook Inc., Bloomington, IL) is advanced into the pericardial space. In cases in which spontaneous circulation is restored, patients are transported to an operating room if indicated.

Statistical Analysis

The data are presented as means ± SD. The Mann-Whitney U test or the χ^2 test was used to compare data in the two groups using the statistical software program StatView-J 5.0, (SAS Institute Inc., Cary, N.C.).

RESULTS

BSP was effective in all cases but PCD was ineffective in five cases because of clotting in the pericardium ($p = 0.260$). Ten patients (BSP, 4; PCD, 6; $p = 0.077$) survived after emergency surgery (n = 8) or conservative treatment (n = 2). No complication was observed in the BSP group but there were five critical complications and three infeasible drainage complications in the PCD group ($p = 0.146$) (Fig. 2). Right ventricular puncture (n = 2) caused by PCD resulted in one death and one open repair after BSP as a second intervention. Acute occlusion of percutaneous drainage tube (n = 3) resulted in two deaths and one emergency thoracotomy (Table 2).

DISCUSSION

Many reports have discussed methods to relieve cardiac tamponade, but mainly in elective cases caused by pericardial effusion.[1–3,6–11] Representative methods of initial management are percutaneous pericardial catheter drainage (PCD)

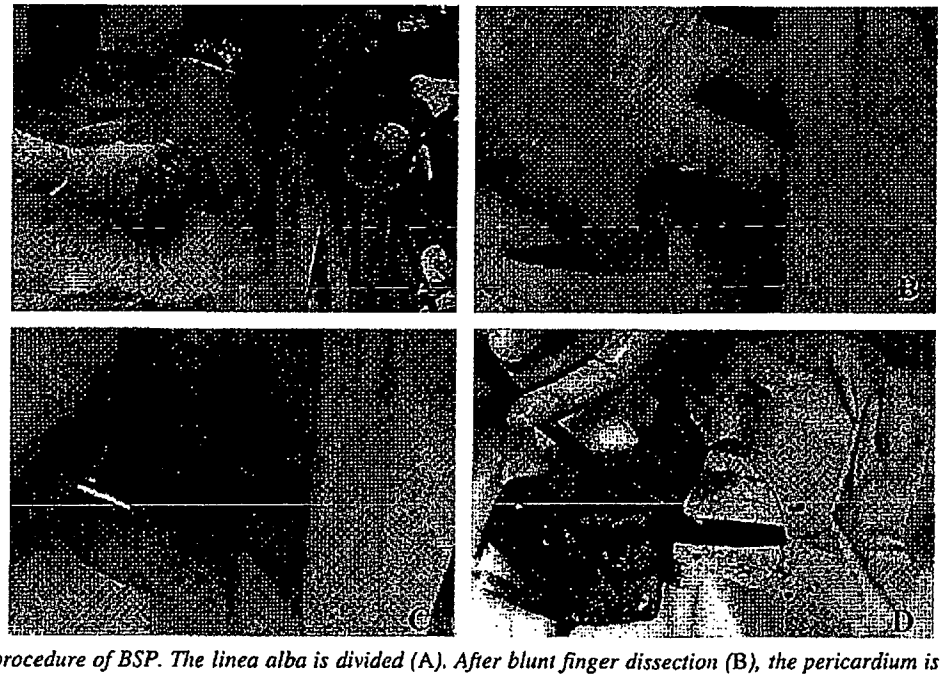

Fig. 1. *Operative procedure of BSP. The linea alba is divided (A). After blunt finger dissection (B), the pericardium is cut by scissors (C). A drainage tube is placed in the pericardium (D).*

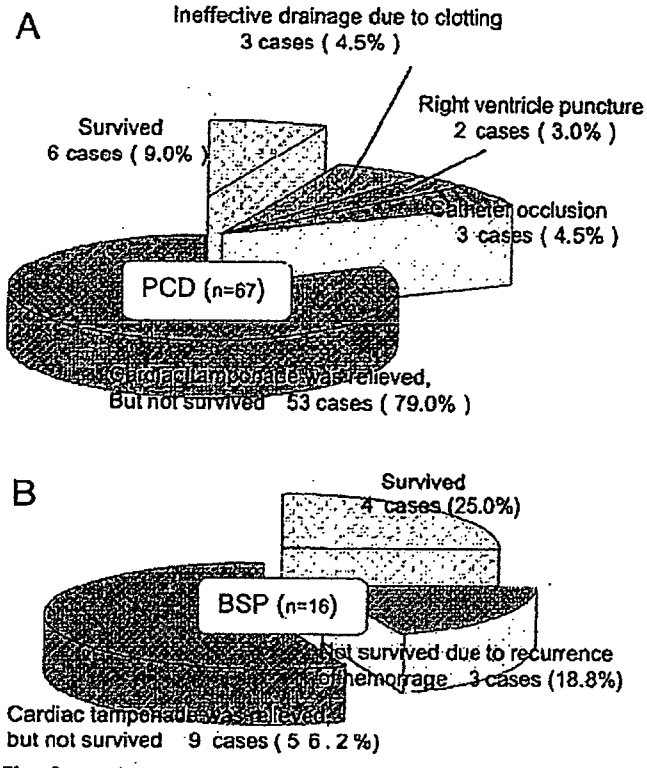

Fig. 2. *Results of percutaneous pericardial catheter drainage (A) and BSP (B). BSP was effective in all cases but PCD was ineffective in five cases (p = 0.260). Ten patients survived (BSP, 4; PCD, 6; p = 0.077). No complication was observed in the BSP group but there were five critical complications and three infeasible drainage complications in the PCD group (p = 0.146).*

Table 2 Clinical Course of Patients With Complications After PCD

Infeasible drainage (n = 3)	67-yr-old woman with AD died in the ER
	55-yr-old man with MI subsequently underwent BSP died in the ER
	69-yr-old man with MI subsequently underwent ERT died in the ER
RV puncture (n = 2)	76-yr-old woman with AD subsequently underwent BSP in the ER, and survived after open repair in the OR
	72-yr-old woman with MI subsequently underwent BSP in the ER, but died during transportation to the OR
Occlusion of catheter (n = 3)	19-yr-old man with trauma subsequently underwent BSP in the ER, and survived after open repair in the OR
	62-yr-old man with MI subsequently underwent BSP in the ER, but died during preparation of open repair in the ICU
	65-yr-old woman with AD died in the ICU

PCD, percutaneous pericardial catheter drainage; AD, aortic dissection; ER, emergency room; MI, myocardial infarction; BSP, blind subxiphoid pericardiotomy; ERT, emergency room thoracotomy; OR, operating room; ICU, intensive care unit.

and subxiphoid pericardiostomy. Three decades ago, needle pericardiocentesis was performed at the bedside without echocardiographic guidance or hemodynamic monitoring and the risk of life-threatening complications were as high as 20%.[4] However, the Mayo clinic group reported that echocardiographically guided pericardiocenteses could be performed with a total complication rate of 4.7% (major, 1.2%; minor, 3.5%)[2] and Maggiolini et al. reported that it could be done more safely using a probe-mounted needle.[1] On the other hand, some reports have presented better results of subxiphoid pericardiostomy as a method of managing pericardial effusion, not only to relieve cardiac tamponade but also for diagnosis of malignancy and infection.[7–9] Regarding the drawbacks of subxiphoid pericardiostomy, it usually requires general anesthesia and surgically trained (to some extent) physicians and it takes several minutes to perform. According to studies comparing these two methods, subxiphoid pericardiostomy was preferable for elective cases with pericardial effusion and PCD should be employed for emergency cases because of cardiac tamponade.[10,11]

The present study was designed to evaluate our modified subxiphoid pericardiotomy, employed to overcome some of the drawbacks of these two techniques for emergency cases with cardiac tamponade secondary to hemopericardium. Echo-guided PCD can be done immediately in the emergency room and also completely avoids the critical complication of right ventricle puncture if using a special needle carrier that facilitates continuous visualization during pericardial puncture. Nevertheless, needle aspiration cannot guarantee that intrapericardial blood will be successfully drawn in a case of clotting hemopericardium.[4] In such cases, it might often result in not only ineffective pericardial drainage but also right ventricle puncture. On the other hand, conventional subxiphoid pericardiostomy generally demands specialized surgical instruments and can be too time-consuming for emergency cases, such as our present CPA cases. Our modified pericardiotomy guarantees relief of cardiac tamponade secondary to hemopericardium and can be performed in a minute without specialized surgical instruments even during cardiac massage, which seems to be preferable for emergency cases, such as CPA or near CPA.

In cases of acute pericardial hemorrhage after trauma, surgical repair of cardiac injury has been recommended as the definitive treatment.[5,12,13] In particular, patients with penetrating cardiac injury need to be transferred to the operating room after or even before pericardial drainage. However, considering that there was a report of percutaneous catheter pericardial drainage being effective in all cases with hemopericardium,[14] it might be reasonable to observe patients with blunt cardiac injury concomitant with other critical injuries and to only perform PCD to relieve cardiac tamponade. In our department, surgical or cath-

eter pericardial drainages have not been employed in the emergency room for patients with acute hemopericardium whose hemodynamics do not contraindicate transfer to the operating room. However, in cases of CPA because of hemopericardium, pericardial drainage is mandatory to resuscitate those patients. In such a situation, we think that pericardial drainage, especially blunt subxiphouid pericardiotomy, must be the first choice of management before emergency room thoracotomy.[15] In the operating room, median sternotomy allows various kinds of repair of cardiac injury. However, although there are insufficient surgical instruments and no circulation assist system in the emergency room, the color of blood gained by pericardial drainage might provide valuable information about the site of cardiac injury, which might suggest the preferable procedure to be undertaken in the emergency room (median sternotomy or left antero-lateral thoracotomy) for patients who cannot be transferred to the operating room even after pericardial drainage.[16]

Although we have to consider a possible bias in this study because only board certified surgeons performed blind subxiphoid pericardiotomy and because of the limited number of patients, our modified pericardiotomy seems to be safe and effective for emergency hemopericardium. In conclusion, blunt subxiphoid pericardiotomy could be a treatment of choice for critical acute hemopericardium. Percutaneous catheter drainage for hemopericardium could not avoid critical complications because of clotting in the pericardium in some cases.

REFERENCES

1. Maggiolini S, Bozzano A, Russo P, et al. Echocardiography-guided pericardiocentesis with probe-mounted needle: report of 53 cases. *J Am Soc Echocardiogr.* 2001;14:821–824.
2. Tsang TS, Enriquez-Sarano M, Freeman WK, et al. Consecutive 1127 therapeutic echocardiographically guided pericardiocenteses: clinical profile, practice patterns, and outcomes spanning 21 years. *Mayo Clin Proc.* 2002;77:429–436.
3. Marcy PY, Bondiau PY, Brunner P. Percutaneous treatment in patients presenting with malignant cardiac tamponade. *Eur Radiol.* 2005;15:2000–2009.
4. Wong B, Murphy J, Chang CJ, et al. The risk of pericardiocentesis. *Am J Cardiol.* 1979;44:1110–1114.
5. Duncan AO, Scalea TM, Sclafani SJ, et al. Evaluation of occult cardiac injuries using subxiphoid pericardial window. *J Trauma.* 1989;29:955–959.
6. Kabukcu M, Demircioglu F, Yanik E, et al. Pericardial tamponade and large pericardial effusions. *Tex Heart Inst J.* 2004;31:398–403.
7. Palantianos GM, Thurer RJ, Pompeo MQ, et al. Clinical experience with subxiphoid drainage of pericardial effusions. *Ann Thorac Surg.* 1989;48:381–385.
8. Dosios T, Theakos N, Angouras D, et al. Risk factors affecting the survival of patients with pericardial effusion submitted to subxiphoid pericardiostomy. *CHEST.* 2003;124:242–246.
9. Becit N, Unlu Y, Ceviz M, et al. Subxiphoid pericardiostomy in the management of pericardial effusions: case series analysis of 368 patients. *Heart.* 2005;91:785–790.
10. Allen KB, Faber LP, Warren WH, et al. Pericardial effusion: subxiphoid pericardiostomy versus percutaneous catheter drainage. *Ann Thorac Surg.* 1999;67:437–440.
11. McDonald JM, Meyers BF, Guthrie TJ, et al. Comparison of open subxiphoid pericardial drainage with percutaneous catheter drainage for symptomatic pericardial effusion. *Ann Thorac Surg.* 2003;76:811–816.
12. Harris DG, Papagiannopoulos KA, Pretorius J, et al. Current evaluation of cardiac stab wounds. *Ann Thorac Surg.* 1999;68:2119–122.
13. Navsaria PH, Nicol AJ. Haemopericardium in stable patients after penetrating injury: is subxiphoid pericardial window and drainage enough? A prospective study. *Injury.* 2005;36:745–750.
14. Symbas PN, Diorio DA, Tyras DH, et al. Penetrating cardiac wounds. *J Thorac Cardiovasc Surg.* 1973;66:526–532.
15. Naunheim KS, Kesler KA, Fiore AC, et al. Pericardial drainage: subxiphoid vs. transthoracic approach. *Eur J Cardio-thorac Surg.* 1991;5:99–104.
16. Sugimoto S, Yamashita A, Baba M, et al. Pericardial drainage prior to operation contributes to surgical repair of traumatic cardiac injury. *Jpn J Thorac Cardiovasc Surg.* 1999;47:31–35.

Transactions of the Materials Research Society of Japan 31[3] 735-738 (2006)

Influence of Cross-linking on Physicochemical and Biological Properties of Collagen-Phospholipid Polymer Hybrid Gel

Kwangwoo Nam, Tsuyoshi Kimura and Akio Kishida
Institute of Biomaterials and Bioengineering, Tokyo Medical and Dental University Kanda-Surugadai 2-3-10, Chiyoda-ku, Tokyo 101-0062, Japan.
FAX:81-3-5280-8029, e-mail: bloodnam.fm@tmd.ac.jp

To adopt collagen as a biomaterial, collagen should be modified due to disadvantages such as poor mechanical strength and high thrombogenicity. Preparation of collagen-polymer hybrid gel for application as an artificial vascular graft was executed by immobilizing 2-methacryloyloxyethyl phosphorylcholine (MPC) polymer, poly(MPC-*co*-methacrylic acid) (PMA), using *N*-(3-dimethylaminopropyl)-*N'*-ethylcarbodiimide and *N*-hydroxysuccinimide as cross-linkers. In order to alter the density of interchain cross-links (intermolecular bonding) between collagen fibrils and the MPC polymer chains, collagen-polymer hybrid gel was prepared by changing the mole ratio of MPC moiety of PMA. The intra- and interhelical cross-links made the gel thermodynamically stable. The interchain cross-links made the gel mechanically and dimensionally stable by supporting the network structure of the hybrid gel, which is thought to be achieved by connecting collagen fibrils. Enzymatic stability was depending on the density of interchain cross-links, because the adsorption of collagenase was prohibited. Increase in the MPC moiety made the gel cell adhesion property decrease. This implies that the interaction between cells and surface of the hybrid gel is being regulated by the MPC groups, making the hybrid gel much efficient for artificial vascular graft use.
Key words: collagen, phospholipids polymer, cross-link, gel, cell adhesion

1. INTRODUCTION

In order to use collagen for a biomaterial product, the cross-linking of collagen and/or immobilizing synthetic polymer with collagen to is indispensable. Non-treated natural collagen cannot directly be applied to the biological system due to disadvantages such as poor mechanical strength, calcium deposition, and high thrombogenicity. However, the collagen is biocompatible and non-antigenic, synergic with bioactive component, easily modifiable, and available in abundance, which makes it suitable for medical application [1-3]. While keeping the advantageous property of collagen, disadvantageous property should be eliminated or be complemented.

Cross-link method using *N*-(3-dimethyl-aminopropyl)-*N'*-ethylcarbodiimide (EDC) and *N*-hydroxysuccinimide (NHS) was chosen for this study [4,5]. Cross-linking collagen with EDC and NHS makes 'zero-length' amide cross-links between carboxylic acid groups from aspartic and glutamic acid residues, and ε-amino groups from (hydroxy-) lysine residues forming intra- and interhelical cross-link to prepare an EDC/NHS cross-link collagen gel [5]. And, 2-methacryloyloxyethyl phosphorylcholine (MPC) based copolymer, which is known for its excellent biocompatibility [6], was used to cross-link the microfibrils of collagen to produce a hybrid gel having biocompatibility and improved mechanical strength.

In this study, we investigated the network structure of the collagen-phospholipid polymer hybrid gel and the effect to the mechanical strength, thermal stability, dimensional stability, and enzymatic stability against collagenase. Furthermore, the biological property of the collagen gel was examined to evaluate the application as an artificial blood vessel.

2. EXPERIMENTAL

2.1 Preparation of EDC and NHS Cross-linked Collagen Gel

Preparation of EDC and NHS cross-linked collagen gel (E/N gel) was executed by using 0.5wt% collagen type I solution (pH 3, KOKEN, Tokyo, Japan). Collagen solution was fabricated into film. Then the collagen film was immersed into the 0.05M 2-morpholinoethane sulfonic acid (MES) buffer (pH 9) (Sigma, St Louis, USA) containing EDC (Kanto Chemicals, Tokyo, Japan) and NHS (Kanto Chemicals, Tokyo, Japan). The cross-linking procedure was executed for 4 hours at 4°C to make a cross-linked gel (E/N-al gel). After 4 hours, the reaction was stopped and the gel was then washed with 4M of Na_2HPO_4 aqueous solution for 2 hours to hydrolyze any remaining *O*-acrylisourea groups and then with distilled water for 3 day to remove salt from the gel. The molar ratio of each chemical was fixed to EDC:NHS:collagen-carboxylic acid groups=5:5:1.

2.2 Preparation of MPC-immobilized Collagen gel

Preparation of the MPC-immobilized Collagen gel (MiC gel) was executed by using E/N-al gel. poly(MPC-*co*-methacrylic acid) (mole ratio; MPC:methacrylic acid=3:7, PMA30) (Figure 1) was added with EDC and NHS in MES buffer (pH 10) and was pre-activated for 10 minutes before E/N-al gel was immersed. The molar ratio of each chemical was fixed to EDC:NHS:carboxylic acid groups of PMA =5:5:1. The immobilization of PMA to the collagen was continued for 4 hours at 4°C. Then the gel was washed with 4M of Na_2HPO_4 aqueous solution for 2 hours and then with distilled water for 1 day to remove salt from the gel to prepare a salt-free MiC30 gel. To increase the MPC moiety of the collagen-polymer hybrid gel, PMA90 (MPC:methacrylic acid=9:1) was prepared and immobilized to the collagen to make a MiC90 gel.

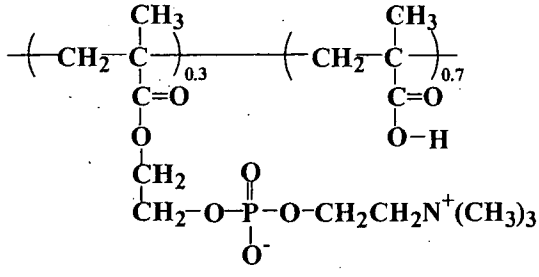

Figure 1.Chemical structure of PMA.

2.3 Surface Characterization

The surface analysis was executed using X-ray photoelectron spectroscopy (XPS; AXIS-HSi, Shimadzu/KRATOS, Kyoto, Japan) and Scanning electron microscopy (SEM; SM-200, Topcon, Tokyo, Japan) Samples which had been cut into small pieces were lyophilized for overnight. The chemical composition of the surfaces of the gel (upper part of the gel) was determined by releasing angle of the photoelectrons fixed at 90°. The morphologies of the gels were observed with a SEM. The razor-blade cut surfaces of respective gels were observed.

2.4 Network Characterization

The shrinkage temperature of the gels were determined using differential scanning calorimeter (DSC; DSC6000, Seiko, Chiba, Japan) in the range of 0°C to 150°C at the scanning rate of 5°C/minute.

Stress-strain curves of respective collagen gels were determined by uniaxial measurements using a tensile strength tester (STA-1150, Orientec, Tokyo, Japan). The sample for the measurement was prepared in the size of 4cm×1cm. The obtained data were changed to stress-strain curve of the samples and the elongation modulus was calculated.

The swelling test of respective samples was executed by cutting lyophilized gels into small pieces and putting into pH aqueous solution at 37°C. The pH of the aqueous solution was controlled to make 7.4. The gels were shaken gently for 24 hours and taken out to measure the changed weight of the sample. Swelling ratio was calculated in order to define the exact swelling phenomenon brought up by water absorption.

2.5 Enzymatic Degradation

The degradation test of the gel samples were executed using collagenase from Clostridiopeptidase histoluticum (EC 3.4.24.3, *Sigma*, St Louis, USA) with collagenase activity of 320 units/mg. In this experiment, collagen gels were immersed into Tris-HCl buffer solution with total concentration of collagenase 100units/mL. The weight of the gels after reaction with collagenase was measured from 1 to 72 hours.

2.6 Cell adhesion test

L-929 cells (mouse fibroblast) were used to evaluate the interaction between collagen gels and the cells. The fibroblasts were culture in Eagle's Minimum Essential Medium (E-MEM; Gibco, NY, USA) supplemented with 10% fetal bovine serum (FBS; Gibco, NY, USA) at 37°C in a 5% CO_2 atmosphere. After treatment with 0.25% trypsin, the cell density was adjusted to 5×10^3 cells/mL and the cells were seeded on the surface. The collagen gels were sterilized by putting gels into ethanol:water 50:50 for 2 hours, than 70:30 for 2 hours, and 100:0 for an overnight before lyophilizing. The lyophilized gels were hydrolyzed with E-MEM for 5 minutes and the E-MEM was disposed just before cell seeding. After 24 hours and 48 hours, the number of adhering cells was determined using lactate dehydrogenase (LDH) assay at 560nm with UV/VIS spectrophotometer (V-560, Jasco, Tokyo, Japan).

3. RESULTS AND DICUSSION

3.1 Surface Characterization

All gels showed XPS signals attributed to carbon in CH_3- or $-CH_2$-, -COC-, C(=O)-, and nitrogen in -CONH- was observed at 285, 286.6, 288.5, and 400.8eV, respectively. A phosphorus peak and one nitrogen peak in $-N^+(CH_3)_3$ was observed at 134eV and 403.2eV, respectively, indicating that PMA was properly cross-linked collagen [6]. Figure 2 shows the images of the outer surface (upper part of the gel) and razor blade-cut surface (cross-section) morphology of respective collagen gels observed with SEM. All outer surfaces that are immobilized with PMA show non-porous homogenous structure. When the razor-cut surface was observed, relatively porous (or hollow) layer that is composed of many thin plates, and non-porous (or dense) layer was seen. Hollow layer is thought be the uncross-linked collagen (a collagen gel that is prepared under pH 9.0 MES buffer without any cross-linker; Uc gel). or intra- and interhelically cross-linked collagen layer. The non-porous layer representing PMA is deposited on the collagen layer and the thickness increases as more PMA is adopted. However, we are not sure yet how the deposited layer would affect the physical property of the hydrogel. We are working on this and would be reported soon.

3.2 Network Characterization

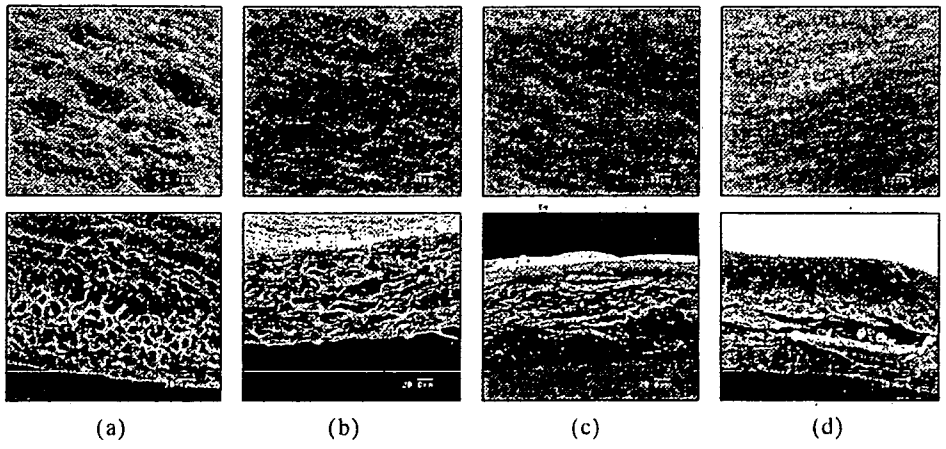

Figure 2. SEM images of collagen gels. (a) Uc gel, (b) E/N gel, (c) MiC90 gel, and (d) MiC30 gels. Upper images imply the outer surface and below images indicate the razor-cut surface of the gels.

Table I shows the change of the shrinkage temperature (T_s) of each collagen gels. The cross-linking brought the increase in the T_s. And the T_s would increase further as the PMA is immobilized, but would never cross 85°C. Since the denaturization temperature is the endothermic transition of the triple helix of the collagen molecules to the random coil, it is believed that intra- and interhelical cross-link controls the T_s [7]. When the higher amount of EDC and NHS was used, the T_s would increase up to 83°C (data not shown). This implies that the increase in the T_s is not due direct connection between collagen microfibrils and polymer chain but due to complexity of the network. So, the stability of the collagen gels against temperature is dependant not only on intra- and interhelical cross-links, but also on the density of the network.

Table I. Shrinkage temperature of respective collagen gels.

Sample	Shrinkage temperature (°C)
Uc gel	56±8
E/N gel	74±3
MiC90	76±3
MiC30	84±4

The elongational modulus increases as PMA is immobilized, indicating it is the interchain cross-link that reinforces the mechanical strength. The elongational modulus of MiC gels measured at 1% strain and 8% strain showed that approximately 10~13 times increase compared to Uc-gel while that of E/N gel showed approximately 5 times increase. This indicates that the network is much denser for MiC gels, which directly affected the mechanical strength.

All collagen gels showed 1.4~2 times increase in elongational modulus at 8% strain compared to that of at 1% strain, indicating soft tissue viscoelastic behavior can be maintained after immobilizing with PMA. So, biomaterial possessing biological property can be obtained.

Figure 3 shows the swelling of the respective gels under pH 7.4. For uncross-linked gel, the gel dissolved under pH 2.1, while swelled approximately 1400% under pH 7.4. When collagen gels absorb water, the triple helix structure is known to turns to random coil conformation, because collagen peptide chains increases accessibility to hydration. In the neutral and alkaline pH conditions, collagen film would be stabilized by forming entanglement of fibrils formed by hydrophobic and electrostatic bonds.

E/N-al gels shows swelling ratio of 320% under pH 7.4. As mentioned earlier, EDC and NHS is known to be bring inter- and intrahelical cross-links, holding the α-helices together tightly. However, its low cross-linking density due to high free amine group contents makes the gel to swell high.

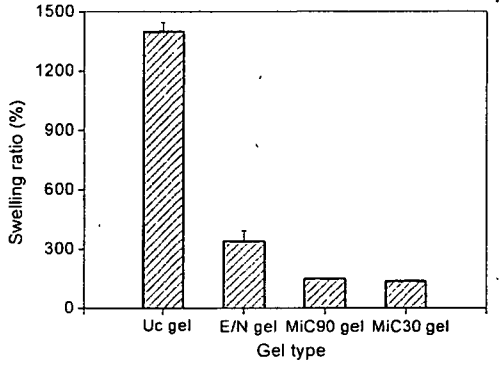

Figure 3. Swelling ratio of respective collagen gels in pH 7.4

MiC gels shows much suppressed swelling ratio. The decrease in the swelling ratio comparing to E/N gel indicates that the dense network has formed. Denser network between collagen and PMA is thought to be formed by interchain cross-links by connecting microfibrils together, increasing the toughness of the collagen gel. Furthermore, the high mechanical strength of the hybrid gel is suppressing the absorption of water, leading to low swelling ratio

3.3 Enzymatic Degradation

Figure 4 shows the degradation of collagen gels caused by the activation of collagenase in Tris-HCl buffer. Collagen gel would be degraded once it encounter with collagenase. Collagenase would cleave the helical segment, which makes the collagen gels to hydrolyze. Collagenase is known to absorb onto the collagen fibers once it penetrates into the fiber [7]. Our study shows that the collagen gel that is not cross-linked would be degraded within 2 or 3 hours. Cross-linking the collagen with EDC and NHS would maintain the helical structure firmly, extending the complete degradation time from 3 hours to 24 hours. And as mentioned previously, the E/N-al gel possesses higher intra- and intercross-link chains, making the gel to endure longer time against collagenase.

MiC gels showed higher stability against collagenase. The network of the collagen gel is thought to be denser than E/N gel, as described previously. For E/N gels, the absorption of collagenase eventually made it to be dissociated within 24 hours. On the other hand, MiC gels possess interchain cross-link, which links the microfibrils and the PMA chains, making the gel to swell much lower. And the cleavage by collagenase would be prevented by the PMA-collagen network which links fiber and polymer chain together, shielding the helices

Comparing the degradation rate between MiC gels, we can see that as MPC ratio increases, the degradation is much faster. This is because the network of the MiC90 is thought to be much sparse than MiC30, due to low mole ratio of methacrylic acid moiety. This makes the space between collagen and PMA larger, resulting in higher water absorbance.

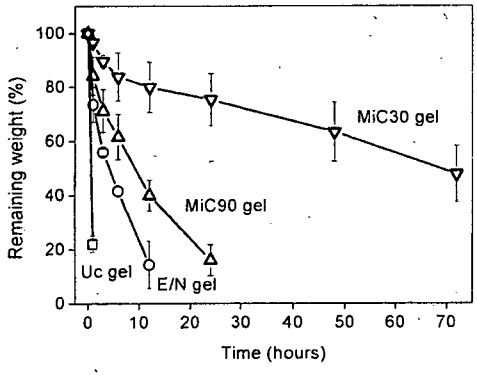

Figure 4. Degradation of collagen gels by collagenase in Tris-HCl buffer (pH 7.4) at 37°C.

3.4 Cell Adhesive property

When the number of adhered cells after 24 hours and 48 hours were compared among the collagen gels, and those with PMA immobilized on collagen gels were much lower than without PMA. This is clearly due to PMA polymer covering the surface of the collagen gel. The number of cell adhered on the surface decreased as the moiety of MPC unit increased. The difference between number of adhered cell on the surface after 24 and 48 hours was compared, the increase in the number of cells was observed for collagen gels. However, for MiC gels, increase was suppressed. Polymer immobilized on the collagen blocks the interaction between fibroblast and collagen, which is known to be the most decisive factor for cell adhesion [8].

4. CONCLUSION

The preparation of MiC gel was successfully achieved. Immobilization of MPC polymer made the gel tougher and stable. We could confirm that the stress-strain responded as generally observed for soft biological materials. Increase in the MPC unit brought the higher swelling, which lead to the faster degradation by collagenase. It is thought that the higher amount of adopted PMA have caused the formation of sparse cross-link network, which in turn make the surface of the MiC gel full of MPC head groups, reducing cell adhesion ability.

The increase in the MPC unit would bring higher biocompatilibty, while increase of MA unit would allow increment of mechanical strength. As the concentration of MPC increased, it is thought that the biocompatibility would increase but toughness decrease.

ACKNOWLEDGEMENT

This study was financially supported by Grant from the research on Health Science focusing on Drug Innovation (KH61060) of the Japan Health Sciences Foundation and Health and Labour Sciences Research Grants.

REFERENCES

[1] W. Friess, *Eur. J. Pharm. Biopharm.*, **45**, 112-136 (1998).
[2] K. Fujioka, M. Maeda, T. Hojo, and A. Sano, *Adv. Drug Del. Rev.*, **31**, 247-266 (1998).
[3] C.H. Lee, A. Singla, and Y. Lee, *Int. J. Pharma.*, **221**, 1-22 (2001).
[4] L.H.H. Olde Damink, P.J. Dijkstra, M.J.A. van Luyn, P.B. van Wachem, P. Nieuwenhuis, and J. Feijen, *Biomaterials*,**17**, 765-773 (1996).
[5] M.J.B. Wissink, R. Beernink, J.S. Pieper, A.A. Poot, G.H.M. Engbers, T. Beugeling, W.G. van Aken, and J. Feijen, *Biomaterials*, **22**, 151-163 (2001).
[6] K. Ishihara, T. Ueda, and N. Nakabayashi, *Polym. J.*, **22**, 355–360 (1990).
[7] R. Zeeman, P.J. Dijkstra, P.B. van Wachem, M.J. van Luyn, M. Hendriks, P.T. Cahalan, and J. Feijen, *Biomaterials*,**20**, 921-931 (1999).
[8] J. Watanabe and K. Ishihara, *Artif Organs*, **27**, 242-248 (2003).

(Received January 31, 2006;Accepted June 2, 2006)

systemic administration. This is achieved with a hydrophilic polymer of which polyethylene glycol (PEG) has been found to be best. Targeting cell-surface receptors is an attractive concept to achieve specific binding and internalisation of the liposome. To this end, cell-binding ligands are displayed from the surface of the liposome. The common denominator for these ligands is that their cell receptor targets are over-expressed in tumours.

We are developing a post-modification methodology for coupling cell or tissue targeting moieties onto liposomes via chemioselective oxime bond formation. Thus, liposomes comprising a highly nucleophilic aminoxy-functionalised lipid are formulated. The aminoxy lipid readily reacts with aldehyde functionalised targeting ligands in aqueous conditions forming a stable oxime bond conjugated targeted liposome.

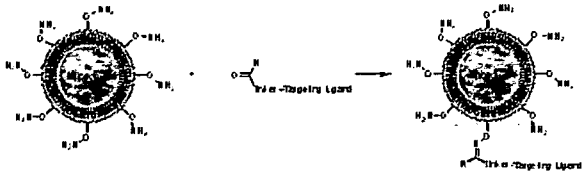

A peptide displaying the RGD sequence was selected as the targeting ligands to validate our post-coupling methodology. A cyclic RGD peptide conjugate has been successfully synthesised using a combination of solution- and solid-phase synthesis. Additionally, control RGE peptide and PEG linker conjugates have been prepared. All the ligands terminate in an aldehyde functional group separated from the targeting moiety by a PEG linker.

The couplings between the RGD conjugate and aminoxy liposomes in water at pH ~4 were shown to be efficient, simple and reproducible. In vitro HUVEC cell uptake studies show a definite targeted uptake of the RGD-targeted liposomes relative to appropriate control liposomes.

193. Gene Transfection Using Inorganic Particle/PVA/DNA Complexes Prepared by Ultra High Pressure Technology

Tsuyoshi Kimura,[1] Kwangoo Nam,[1] Sihngo Mutsuo,[2] Hidekazu Yoshizawa,[2] Masahiro Okada,[3] Tsutomu Furuzono,[3] Toshiya Fujisato,[4] Akio Kishida.[1]

[1]Institute of Biomaterials and Bioengineering, Tokyo Medical and Dental University, Tokyo, Japan; [2]Department of Environmental Chemistry and Materials, Okayama University, Okayama, Japan; [3]Department of Biomedical Engineering, National Cardiovasucular Center Research Institute, Osaka, Japan; [4]Department of Regenerative Medicine and Tissue Engineering, National Cardiovasucular Center Research Institute, Osaka, Japan.

Various non-viral gene systems, such as naked DNA, lipoplexes, micelles and polyplexes, have been developed for effective and safe gene delivery into target cells. Although cationic compounds were employed as gene carriers due to the ability of complex formation with DNA electrostatically and effective gene transfer into cells, the intrinsic cytotoxicity of them is essential problem in non-viral gene delivery system. Therefore, we have tried the development of DNA complex with non-ionic, water soluble polymers via hydrogen bond using ultra high pressure (UHP) technology because the inter-, intra-molecular week hydrogen bonding interaction was empathized with high pressure process. Previously, polyvinyl alcohol (PVA) was utilized as the model hydrogen bonding polymers, and the PVA/DNA complexes were obtained by UHP treatment. Although the PVA/DNA complexes were up-taken by cells, a little enhancement of gene expression was observed using them. In this study, we hypothesize that inorganic particles, such as calcium phosphate (CP), calcium carbonate and hydroxy apatite (HAp), promote the endosomal escape of transferred DNA because the inorganic particles are dissolved under low pH condition in endosome vesicles and then the rupture of endosome is induced by osmotic shock. We performed the development of inorganic particle/PVA/DNA complexes using UHP technology. Plasmid DNAs encoding enhanced green fluorescent protein (EGFP) gene or luciferase gene under CMV promoter were used. Nano-HAps having the average diameter of 50nm were synthesized by modified micro-emulsion method. Nano-HAp was dispersed ultrasonically in PVA solution and then mixed with DNA solution. CP/DNA complexes were prepared by general method and mixed with PVA solution. Their mixtures were treated under 10000 atmospheric pressures at 40 degree for 10min. By SEM observation, the irregular surface of inorganic particles/PVA/DNA complexes was observed, indicating the encapsulation of inorganic particles in PVA/DNA particle. The nano-HAp/PVA/DNA complexes showed a higher transfection activity than DNA complexes with nano-HAp or PVA. With CP/PVA/DNA complexes, also, the transfection activity increased several fold than the PVA/DNA complexes. These results indicate the utility of the inorganic particle/PVA/DNA complexes prepared by the UHP treatment for DNA delivery.

194. Development of Novel DNA Formulations Based on Polymers and Cyclodextrin for Gene Delivery to the Muscle

Caroline Roques,[1,2] André Salmon,[1] Marc Y. Fiszman,[1] Elias Fattal,[2] Yves Fromes.[1]

[1]Gene Therapy Lab, Institut de Myologie - INSERM u582, Paris, France; [2]CNRS UMR 8612, University of Paris - Faculty of Pharmacy, Chathenay-Malabry, France.

So far gene transfer to the muscle has mainly been based on viral vectors, given their efficiency to transfer DNA in vivo. However, virus-derived vectors have numbers of limitations, such as insert size, tissue specificity or immunogenicity, therefore restricting the possibilities of repeated administrations. After intramuscular injection, major hurdles remain tissue diffusion and intracellular entry.

To improve these parameters with reference to naked DNA, our approach consisted in designing synthetic vectors. The first step intended to condense and protect plasmid DNA (pCMV-βGal, Invitrogen) through its association with various polymers differing by their charge, i.e. Polyethyleneimine (PEI, Sigma), Tetronic 304 (BASF) and PE6400 (BASF). For each polymer/DNA formulation, the morphological properties of the vectors were assessed by cryo-Transmission Electron Microscopy, their size by Dynamic Light Scattering and their zeta potential by Laser Doppler Velocimetry. Characterization revealed a great diversity of objects in terms of size, shape and zeta potential.

In vivo toxicity and efficiency of the systems were also evaluated after intramuscular injections into tibialis anterior and quadriceps muscles of wild type Syrian hamsters. X-Gal revelation and Haematein/Eosin staining were then performed on serial sections of each muscle. These experiments highlighted the extremely high cytotoxicity of PEI/DNA complexes towards skeletal muscle. On the contrary, no significant lesions were detected after injection of PE6400/DNA or Tetronic/DNA formulations. Both systems did significantly improve transfection with reference to naked DNA.

In order to promote cellular entry of the DNA, a second step in our study consisted in combining the previous polymeric vectors with randomly methylated beta-cyclodextrin (Rameb) since this compound has demonstrated its ability to destabilize the cell membrane through cholesterol complexation. In vivo toxicity of Rameb after intramuscular injection has been assessed as well as efficiency when associated to polymer/DNA formulations. Addition of Rameb to the polymeric vectors did not allow a significant increase

Optimization of amino group density on surfaces of titanium dioxide nanoparticles covalently bonded to a silicone substrate for antibacterial and cell adhesion activities

Masahiro Okada,[1] Shoji Yasuda,[1] Tsuyoshi Kimura,[1] Mitsunobu Iwasaki,[2] Seishiro Ito,[2] Akio Kishida,[1] Tsutomu Furuzono[1]

[1]*Department of Bioengineering, National Cardiovascular Center Research Institute, 5-7-1 Fujishirodai, Suita, Osaka 565-8565, Japan*

[2]*Department of Applied Chemistry, Faculty of Science and Engineering, Kinki University, 3-4-1 Kowakae, Higashiosaka, Osaka 577-8502, Japan*

Received 7 April 2005; revised 14 June 2005; accepted 20 June 2005
Published online 1 September 2005 in Wiley InterScience (www.interscience.wiley.com). DOI: 10.1002/jbm.a.30513

Abstract: A composite consisting of titanium dioxide (TiO_2) particle, the surface of which was modified with amino groups, and a silicone substrate through covalent bonding at their interface was developed, and antibacterial and cell adhesion activities of the composite were evaluated. The density of the amino groups on the TiO_2 particle surface was controlled by the reaction time of the modification reaction. The degradation rate of CH_3CHO in the presence of the TiO_2 particles under UV irradiation decreased with an increase in the amino group density on the TiO_2 surface. On the other hand, the number of L929 cells adhering on the TiO_2/silicone composite increased with an increase in the amino group density. From the above two results, the optimum density of amino groups for both photoreactivity and cell adhesiveness was estimated to be 2.0–4.0 molecules/nm^2. The optimum amino group-modified TiO_2/silicone composite sheet (amino group density, 3.0 molecules/nm^2) showed an effective antibacterial activity for *Escherichia coli* bacteria under UV irradiation. © 2005 Wiley Periodicals, Inc. J Biomed Mater Res 76A: 95–101, 2006

Key words: titanium dioxide; antibacterial activity; composite; covalent bonding; cell adhesion

INTRODUCTION

Since Fujishima et al.[1] reported water cleavage on photoexcited titanium dioxide (TiO_2) electrodes, TiO_2 has attracted great interest in environmental fields such as air and water purification, because the electron and hole created by photoexcitation of TiO_2 can reduce or oxidize several chemical species adsorbed on the TiO_2 surface.[2–5] The antibacterial activity or cytotoxicity, which is expected to be applicable to biology and medicine, of photoexcited TiO_2 has also been shown.[6–8] In addition, the effect of TiO_2 particles on animals has been investigated from the viewpoint of genetic toxicity; Bischoff et al.[9] and Bernard et al.[10] reported the nontoxicity of TiO_2 particles to animals. TiO_2 has, therefore, also attracted much interest in medical fields.

Recently, we developed a novel inorganic/organic nanocomposite for a percutaneous device: a flexible silicone elastomer, the surface of which was modified with bioactive hydroxyapatite (HAp) nanoparticles through covalent bonding.[11] When this novel composite material is percutaneously implanted into a living body, it is expected to prevent initial germ infection from the outside because the HAp particles existing on the surface of the composite improve adhesion between living tissues and the composite. Actually, the novel composite showed good tissue adhesiveness in animal implant tests.[12] Furthermore, in a previous article,[13] we tried to incorporate two functions, that is, bioactivity and photoreactivity, into a percutaneous device by using TiO_2 particles. Such a system is expected to prevent damage by the antibacterial activity of photoexcited TiO_2 when a germ infection unfortunately occurs after implantation. In order to make covalent linkage between TiO_2 particles and a silicone

Correspondence to: T. Furuzono; e-mail: furuzono@ri.ncvc.go.jp

Contract grant sponsor: New Energy and Industrial Technology Development Organization (NEDO), Japan

substrate and to promote cell adhesion on TiO_2 particles, the surfaces of TiO_2 particles were modified with an amino group-terminated silane coupling agent. Although the composite showed good cell adhesiveness, the photoreactivity was approximately 30 times lower than that of the original TiO_2, which should be due to high coverage of the TiO_2 surface by amino groups.

In this article, in order to develop a TiO_2/silicone composite having both antibacterial and cell adhesion activities, the amino group density on the TiO_2 particle surface was optimized. Antibacterial activity test of the composite was additionally conducted in order to evaluate the functionality of the amino group-modified TiO_2/silicone composite.

MATERIALS AND METHODS

Materials

Anatase TiO_2 particles with an inter-diameter of 200–300 nm and a specific surface area of 5.0 m^2/g were kindly donated by Ishihara Sangyo Co., Ltd. (Osaka, Japan). A silicone sheet (Shin-Etsu Polymer Co., Tokyo, Japan) with a thickness of 0.3 mm was purified by methanol with a Soxhlet extractor. Acrylic acid (AAc; Nacalai Tesque, Inc., Kyoto, Japan) was purified by vacuum distillation. γ-Aminopropyltriethoxysilane (γ-APS; Shin-Etsu Chemical Industries Co., Tokyo, Japan) was used without further purification.

Introduction of amino groups on the surfaces of the TiO_2 particles

TiO_2 particles, 5.0 g, after drying at 120°C for 24 h were added to 150 mL of anhydrous toluene in a 300-mL three-necked flask equipped with an inlet of N_2, a reflux condenser, and a half-moon type stirrer. After the temperature of the mixture was raised to 30°C, γ-APS was injected into the mixture, and it was stirred at 30°C for different reaction periods. After the reactions, the TiO_2 particles were washed with toluene and acetone by centrifugation to remove any unreacted silane coupling agent and dried at 60°C for 24 h. The density of amino groups on the surfaces of the TiO_2 was calculated from the specific surface area of the particles and the weight percentage of carbon atoms in the modified particles. The weight percentage of carbon atoms was measured with an elemental analyzer (EMIA-110; Horiba Ltd., Kyoto, Japan), assuming that all of the amino groups existed on the particle surfaces.

Photoreactivity of the amino group-modified TiO_2 particles

The photoreactivity of the amino group-modified TiO_2 was evaluated by the degradation rate of CH_3CHO. The initial concentration of CH_3CHO in a Pyrex reaction vessel (760 mL) was fixed at approximately 300 ppm in air. UV/Vis light (wavelength, >300 nm) was irradiated with a Xe lamp (HX-500; Wacom Electric Co., Ltd, Tokyo, Japan) at 2000 $\mu W/cm^2$ onto the samples (0.07 g) after the adsorption equilibrium of CH_3CHO in the reaction vessel had been achieved. The concentration of CH_3CHO was determined by a gas chromatograph (GC-8APT; Shimadzu Co., Kyoto, Japan) equipped with an f.i.d. column Shincarbon A. The rate constant for the degradation of CH_3CHO was calculated from the first-order rate equation.[14,15]

TiO_2/silicone composite

First, graft-polymerization of AAc was conducted on the surface of the silicone sheet.[11] The silicone sheet was initially treated by corona-discharge to donate radicals on the surface. The sheet was immersed into a 10 wt% AAc aqueous solution in 50-mL thick-walled tubes, and the tubes were subsequently degassed and sealed. Polymerization was conducted at 60°C for 30 min, and the poly(AAc)-grafted silicone sheet was rinsed with a great deal of hot water to remove homopolymers adsorbed physically. Surface-treated sheets possessing a poly(AAc)-grafted density of 10–20 $\mu g/cm^2$ were used in this study.

In order to adsorb the modified TiO_2 particles onto the poly(AAc)-grafted silicone sheet, 0.2 g of the particles were suspended in 50 mL of water, and the sheet was soaked in the suspension for 1 h at room temperature. After the adsorption, the sheet was heated at 180°C for 2 h in a vacuum for a reaction between the amino groups on the TiO_2 particles and the carboxyl groups on the poly(AAc)-grafted silicone sheet. The composite was washed by using an ultrasonic generator for 3 min (output, 20 kHz; 35 W) in water to remove the particles physically adsorbed on the sheet. In the case of the original TiO_2 particles, the ultrasonic cleaning was not conducted because all of the particles were just physically adsorbed on the sheet. The surface of the composite was observed by scanning electron microscopy (SEM; JSM-6301F, JEOL Ltd., Tokyo, Japan), and the surface-coverage ratio by TiO_2 particles was determined from SEM images. In following experiments, the TiO_2/silicone composite sheets, whose surface-coverage ratio by TiO_2 particles were 50–60%, were used (Fig.1).

Cell adhesion

L929 mouse fibroblast cells were placed onto the TiO_2/silicone composite in 24-well multiplates at 1×10^5 cells/well in a culture medium consisting of an α-minimum essential medium (α-MEM; Gibco Laboratories Inc.) and 10% fetal bovine serum, and incubated at 37°C for 24 h. For SEM observation, the cells were dehydrated with aqueous ethanol (30–100%) and 100% *n*-butanol for 5 min at room temperature step by step. The samples were subsequently lyophilized and coated with gold. The number of L929 cells on the sample substrate was counted from SEM images. As a control sample, the poly(AAc)-grafted-silicone sheet, on

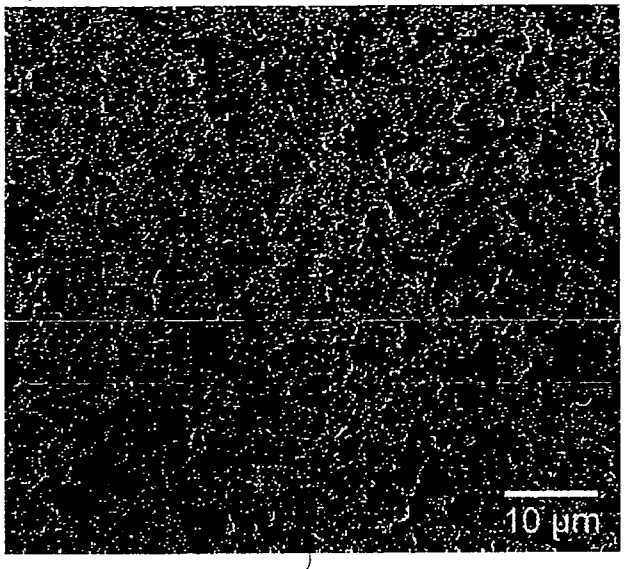

Figure 1. A typical SEM photograph of a surface of amino-group-modified TiO_2/silicone composite sheet, showing a 60% covered surface by the modified TiO_2 particles (amino group density, 3.0 molecules/nm^2).

which the original TiO_2 particles were physically adsorbed, was used.

Cytotoxicity assay

A cytotoxicity assay for the TiO_2/silicone composite was conducted as follows. One gram of the composite was cut into small pieces and added into 10 mL of cell culture medium (α-MEM with 10% fetal bovine serum), and the mixture was incubated at 37°C for 24 h in darkness. After L929 cells (initial number, 1×10^4 cells/well) were precultured at 37°C for 24 h, the culture medium was replaced by the medium exposed to the samples, and the cells were further incubated for another 24 h at 37°C. The number of cells was counted with a hemacytometer after trypsinization and dilution. As a control, the same procedure was conducted with a nontreated medium.

Antibacterial activity

E. coli bacteria (NBRC 3301 strain; Biological Resource Center, Biotechnology Center, National Institute of Technology and Evaluation, Chiba, Japan), precultured at 37°C for 16 h, were washed by centrifuging at 4000 rpm, resuspended, and diluted to 1×10^5 cells/mL with a physiological salt solution. The composite sheets were placed in 24-well multiplates, and then 1 mL of the *E. coli* suspension was pipetted into each well. This system was irradiated with a 4-W back-light bulb (wavelength, 360 nm; 470 μW/cm^2; FL15 BL-B; National Panasonic) at 37°C for 2 h. After the irradiation, 100 μL of each *E. coli* suspension was pipetted out and incubated in a nutrient agar medium at 37°C for 16 h, and the number of viable bacteria was counted. As a control test, the above procedure was conducted without the composite sheet or without UV irradiation.

Statistical analysis

Data resulting from cytotoxicity assays and antibacterial activity tests are presented as means ± SD for mean ($N = 4$). Statistical comparisons were performed with the use of a Student's t test. The level of statistical significance was defined as $p < 0.05$.

RESULTS AND DISCUSSION

The TiO_2 particles were chemically modified with an amino group-terminated silane coupling agent at 30°C for different reaction time. In the previous article,[13] modification with amino groups was confirmed by FT-IR. Figure 2 shows the density of amino groups on the surfaces of the TiO_2 particles after modification at 30°C for different reaction times. The density of the amino groups was determined from the specific surface area of the TiO_2 particles and the carbon content measured by elemental analysis. In order to determine the amino group density, the nitrogen content was not used because it was below the detection limit. The density of the amino groups incorporated on the particle surfaces drastically increased within 1 h, gradually increased with an increase in the reaction time, and then almost reached a plateau at about 5 molecules/nm^2. Judging from the fact that the theoretical density of the OH groups on the anatase TiO_2 surface is 12–14 molecules/nm^2, which is estimated from lattice constant,[16] and that each silane coupling agent reacts with less than three OH groups, it is estimated

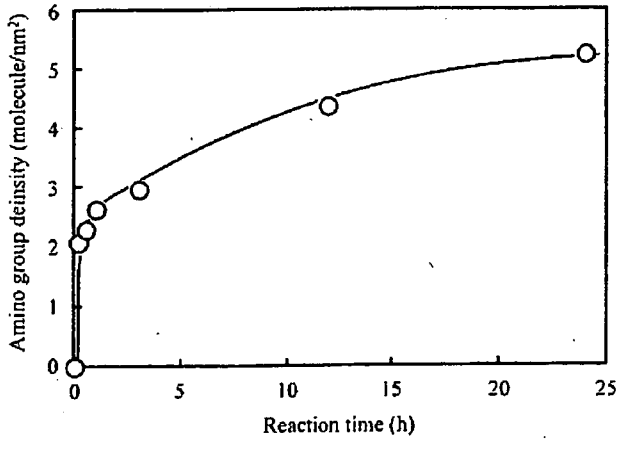

Figure 2. Amino group densities on the TiO_2 particle surfaces after modification at 30°C for different reaction times.

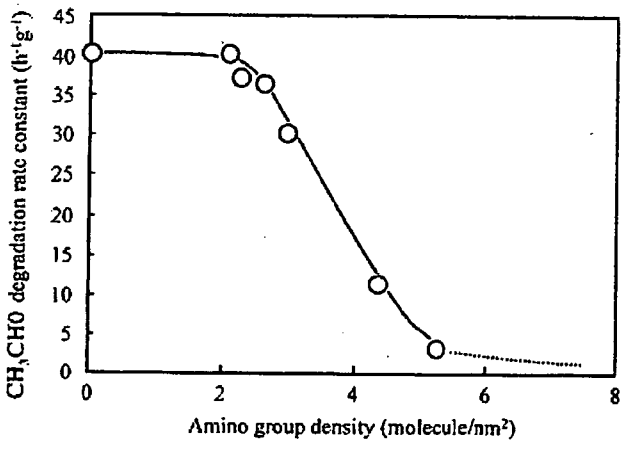

Figure 3. Relationship between the amino group density on the TiO_2 particle surfaces and the degradation rate constant calculated from the decrease of CH_3CHO concentration by UV irradiation (>300 nm; 2000 $\mu W/cm^2$; 2 h).

that the modified TiO_2 particle surface consisted of not only an amino group-donated surface but also an intact TiO_2 surface, at least in the case of an amino group density of <4 molecules/nm^2.

The photoreactivity of the modified TiO_2 was evaluated by the degradation rate of CH_3CHO. In the previous article,[13] although the anatase phase of the TiO_2 particles did not change after the reaction between the silane coupling agent and the OH groups on the outermost surface of the particle, the photoreactivity became approximately 30 times lower than that of the original TiO_2, which should be due to high coverage of the TiO_2 surface by silane coupling agents. The high coverage in the previous study should be due to crosslinking reactions among the silane coupling agents at a higher reaction temperature (120°C) than that of this study (30°C). Figure 3 shows the relationship between the density of amino groups on the TiO_2 particle surface and the rate constant calculated from the first-order rate equation[14,15] for CH_3CHO degradation by UV irradiation (wavelength, >300 nm; 2000 $\mu W/cm^2$) within 2 h. The photoreactivity did not change in the case of an amino group density of <2 molecules/nm^2 and drastically decreased with an increase in the amino group density. This result suggests that the decrease of the photoreactivity was due to the suppression of contact between CH_3CHO molecules and the intact TiO_2 surface by the silane coupling agents.

Figure 4 shows the FT-IR spectra of the original TiO_2 and the amino group-modified TiO_2 particles (amino group density, 3.0 molecules/nm^2) before and after UV irradiation (>300 nm; 2000 $\mu W/cm^2$; 2 h). Each sample was heated at 120°C for 24 h before the FT-IR measurement to remove adsorbed water. In the spectrum of the original TiO_2 [Fig. 4(a)], the band at 3692 cm^{-1} is attributed to the OH stretching vibration of the bridge-OH terminal groups on the outermost surface of TiO_2. The peaks at 3300 and 1650 cm^{-1} depend on adsorbed H_2O on the TiO_2. In the spectrum of the TiO_2 after modification with γ-APS [amino group density, 3.0 molecules/nm^2; Fig. 4(b)], the intensity of the band at 3692 cm^{-1}, attributed to the bridge-OH terminal groups of TiO_2, decreased, which corresponded to that reported in the previous article,[13] indicating the reaction of the OH groups with the silane coupling agent. An additional peak is present with respect to the original TiO_2 spectrum at 2928 cm^{-1}, indicating C—H stretching of the organic compound. As compared to the spectrum of the amino group-modified TiO_2 before UV irradiation, that after UV irradiation [Fig. 4(c)] in air did not change, which indicates that the covalent bonding did not cleave under the UV irradiation conditions within 2 h (wavelength, >300 nm; 2000 $\mu W/cm^2$). This result might be due to the slightly larger bonding energy of Si—O (369 kJ/mol) compared to that of C—C (350 kJ/mol) or C—N (291 kJ/mol) and also due to multicoupling between the silane coupling agent and the OH groups on the TiO_2 particles.

The cytotoxicity assays were conducted with the poly(AAc)-grafted silicone sheet, on which the original TiO_2 particles were physically adsorbed, and the amino-group-modified TiO_2/silicone composite (amino group density, 3.0 molecules/nm^2). Figure 5 shows the results. The number of L929 cells after incubation at 37°C for 24 h (total incubation period, 48 h) in the medium, which was exposed to each sample at 37°C for 24 h in darkness, was not statistically significant compared with that after incubation in the nontreated medium (control). This indicates that the original TiO_2/silicone and the amino-group-modified TiO_2/silicone composite sheet had no cytotoxicity to L929 cells.

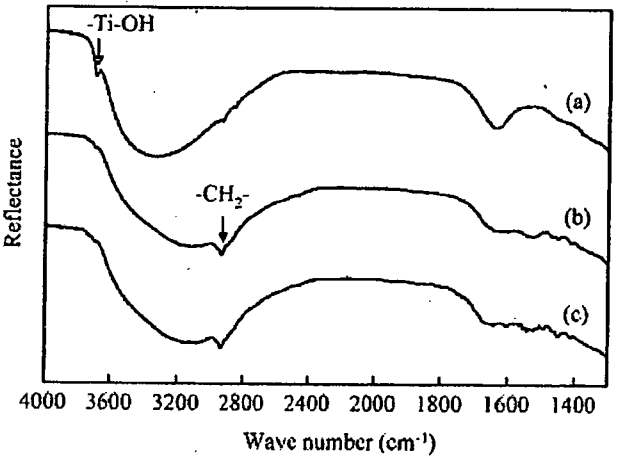

Figure 4. IR spectra of (a) original and (b,c) amino group-modified TiO_2 (amino group density, 3.0 molecules/nm^2) particles (b) before and (c) after UV irradiation (>300 nm; 2000 $\mu W/cm^2$; 2 h).

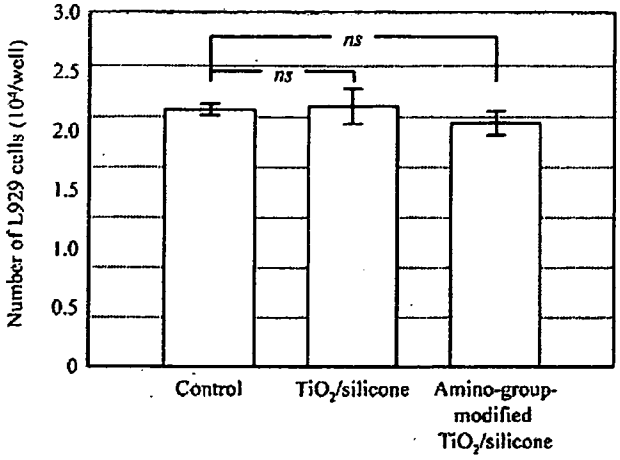

Figure 5. The number of L929 cells after incubation at 37°C for 24 h (total incubation period, 48 h; see Materials and Methods) in the medium exposed to the poly(AAc)-grafted silicone sheet, on which the original TiO_2 particles were physically adsorbed, and the amino-group modified TiO_2/silicone composite sheets (the amino group density, 3.0 molecules/nm^2). Initial number of cells, 1×10^4 cells/well. Error bars represent standard deviations of quadruplicates.

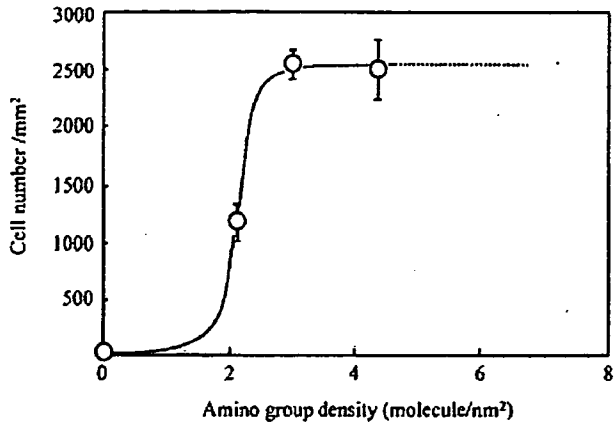

Figure 7. SEM photographs of L929 cells adhering on amino-group modified TiO_2/silicone composite sheets after incubation in 24-well multiplates (1×10^5 cells/well) at 37°C for 24 h. The amino group density on TiO_2 particle surfaces (molecules/nm^2): (a,a') 0; (b,b'); 2.1; (c,c') 3.0. (a,b,c) low magnification; (a',b',c') high magnification.

In order to evaluate the cell adhesion activity of the TiO_2/silicone composite, L929 cells were scattered and incubated on the composite sheet for 24 h at 37°C. Figures 6 and 7 show, respectively, SEM photographs and the number of the L929 cells adhering on the control sample [the poly(AAc)-grafted silicone sheet, on which the original TiO_2 particles were physically adsorbed] and the composite sheet with the TiO_2 having different amino group densities. In the case of the control sample shown in Figure 6(a), few cells adhered. Judging from the cytotoxicity assay shown in Figure 5, the lack of cell adhesion on the control sample was not due to the cytotoxicity of the TiO_2/silicone, but high hydrophilicity of the original TiO_2 surface. On the other hand, the cells dramatically adhered on the composite surface compared with the control sample, and the number of cells adhering on the composite sheet increased with the increase in the amino group density (Fig. 7). This is because cationic groups such as amino groups promote initial cell adhesion and growth.[17] In photographs with higher magnification [Fig. 6(b',c')], the cells elongated their needlelike

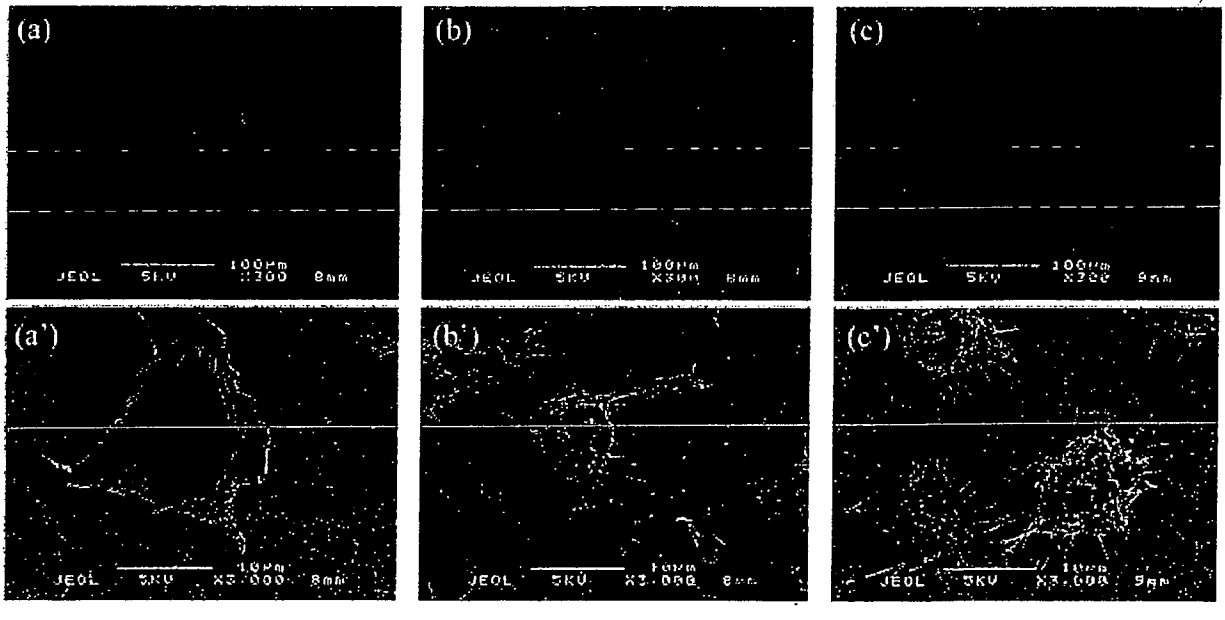

Figure 6. Relationship between the amino group density on the TiO_2 particle surfaces and the number of L929 cells adhering on the TiO_2/silicone composite sheets after incubation in 24-well multiplates (1×10^5 cells/well) at 37°C for 24 h.

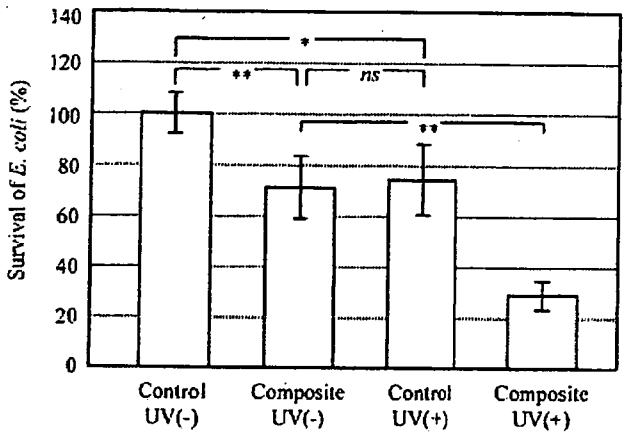

Figure 8. Effect of UV irradiation (360 nm; 470 $\mu W/cm^2$; 120 min) on the number of *E. coli* cells on the amino group-modified TiO_2/silicone composite sheet. The amino group density on the TiO_2 particle surfaces was 3.0 molecules/$nm.^2$ Error bars = SD of quadruplicates ($^*p < 0.05$; $^{**}p < 0.01$).

microspikes restrictedly onto the amino group-modified TiO_2 surface. The microspikes from the cells had no affinity for the bottom of the poly(AAc)-grafted silicone surface having high hydrophilicity[13] and the original TiO_2 particles [Fig. 6(a')].

From the above results shown in Figures 3 and 7, the optimum density of amino groups for both photoreactivity and cell adhesiveness was estimated to be 2.0–4.0 molecules/nm^2. Therefore, the TiO_2/silicone composite consisting of the TiO_2 particles (amino group density, 3.0 molecules/nm^2) was used for the antibacterial activity test. It is worth pointing out that the TiO_2/silicone composite showed the same flexibility as the original silicone sheet, that is, the chemical surface modification with TiO_2 particles showed no mechanical disadvantage, which was similar to the HAp/silicone composite.[12]

The antibacterial activity of the optimum amino group-modified TiO_2/silicone composite (amino group density, 3.0 molecules/nm^2) was estimated from survival ratio of *E. coli* bacteria on the composite sheet after UV irradiation (wavelength, 360 nm; 470 $\mu W/cm^2$; 2 h), which is shown in Figure 8. In the case of the control test after UV irradiation, the direct antibacterial effect of UV rays was slightly observed. On the other hand, in the case of the composite sheet, 29% decrease in the number of *E. coli* bacteria was observed before UV irradiation, and the number of bacteria decreased significantly after UV irradiation (72%). These results indicate a bacteria adsorption onto the optimum amino group-modified TiO_2/silicone composite and effective antibacterial activity by photoexcited TiO_2 under UV irradiation. It is expected that a completely destroying of bacteria will be obtained by optimizing the surface area of the composite sheets and UV irradiation conditions such as wavenumber, intensity, and irradiation time of UV light. It is worth pointing out that the covalent bonding was not cleaved under the UV irradiation (wavelength, >300 nm; 2000 $\mu W/cm^2$; 2 h) as shown in Figure 4. Therefore, the composite developed here is expected to show antibacterial activity under UV irradiation while maintaining tissue adhesiveness.

In conclusion, the amino group density on the TiO_2 particle surface was optimized in order to develop a composite consisting of amino group-modified TiO_2 particles and a flexible silicone sheet through covalent linkage, having both photoreactivity and cell adhesiveness. The photoreactivity of the TiO_2 particles decreased with an increase in the amino group density on the TiO_2 particle surfaces. On the other hand, the number of L929 cells adhering on the composite sheet increased with an increase in the amino group density. Based on the above results, the optimum density of amino groups for both photoreactivity and cell adhesiveness was estimated to be 2.0–4.0 molecules/nm^2, and a composite consisting of TiO_2 particles having that optimum density was developed. Irradiation of UV light onto *E. coli* on the optimum amino group-modified TiO_2/silicone sheet showed an effective antibacterial activity of the composite. The composite developed here could be utilized for elastic percutaneous or subcutaneous devices having good tissue adhesiveness and an antibacterial effect.

References

1. Fujishima A, Honda K. Electrochemical photolysis of water at a semiconductor electrode. Nature 1972;238:37–38.
2. Ollis DF, Pelizetti E, Serpone N. Destruction of water contaminants. Environ Sci Technol 1991;25:1523–1529.
3. Uchida H, Itoh S, Yoneyama H. Photocatalytic decomposition of propyzamide using TiO_2 supported on activated carbon. Chem Lett 1993:1995–1998.
4. Heller A. Chemistry and applications of photocatalytic oxidation of thin organic films. Acc Chem Res 1995;28:503–508.
5. Sitkiewitz S, Heller A. Photocatalytic oxidation of benzene and stearic acid on sol-gel derived TiO_2 thin films attached to glass. New J Chem 1996;20:233–241.
6. Cai R, Kubota Y, Shiumi T, Sakai H, Kashimoto K, Fujishima A. Induction of cytotoxicity by photoexcited TiO_2 particles. Cancer Res 1992;52:2346–2348.
7. Sunada K, Kikuchi Y, Hashimoto K, Fujishima A. Bactericidal and detoxification effects of TiO_2 thin film photocatalysts. Environ Sci Technol 1998;32:726–728.
8. Morioka T, Saito T, Nara Y, Onoda K. Antibacterial action of powdered semiconductor on serotype g Streptococcus mutans. Caries Res 1988;22:230–231.
9. Bischoff F, Bryson G. Tissue reaction to and fate of parenterally administered titanium dioxide. I. The intraperitoneal site in male Marsh-Buffalo mice. Res Commun Chem Pathol Pharmacol 1982;38:279–290.
10. Bernard BK, Osheroff MR, Hofman A, Mennear JH. Toxicology and carcinogenesis studies of dietary titanium dioxide-coated

mica in male and female Fischer 344 rats. J Toxicol Environ Health 1989;28:415–426.
11. Furuzono T, Sonoda K, Tanaka J. A hydroxyapatite coating covalently linked onto a silicone implant materials. J Biomed Mater Res 2001;56:9–12.
12. Furuzono T, Wang P, Korematsu A, Miyazaki K, Oido-Mori M, Kowashi Y, Ohura K, Tanaka J, Kishida A. Physical and biological evaluations of sintered hydroxyapatite/silicone composite with covalent bonding for a percutaneous implant material. J Biomed Mater Res B Appl Biomater 2003;65B;217–226.
13. Furuzono T, Iwasaki M, Yasuda S, Korematsu A, Yoshioka T, Ito S, Kishida A. Photoreactivity and cell adhesiveness of amino-group-modified titanium dioxide nano-particles on silicone substrate coated by covalent linkage. J Mater Sci Lett 2003;22: 1737–1740.
14. Anderson C, Bard AJ. Improved photocatalytic activity and characterization of mixed TiO_2/SiO_2 and TiO_2/Al_2O_3 Materials. J Phys Chem 1997;99:2611–2616.
15. Tada H. Photoinduced oxidation of methylsiloxane monolayers chemisorbed on TiO_2. Langmuir 1996;12:966–971.
16. Morimoto T, Nagao M, Tukuda F. The relation between the amounts of chemisorbed and physisorbed water on metal oxides. J Phys Chem 1969;73:243–248.
17. Rosen JJ, Gibbons DF, Culp LA. In: Andrade JD, editor, ACS Symposium Series 31. Washington, DC: American Chemical Society; 1976. p 329–343.